Colloids and Surfaces A 549 (2018) 164–173

Contents lists available at ScienceDirect

Colloids and Surfaces A

journal homepage: www.elsevier.com/locate/colsurfa

Effect of initial droplet shape on the tangential force required for spreading and sliding along a solid surface

Inmaculada Ríos-López[a], Sotiris Evgenidis[a], Margaritis Kostoglou[a], Xenophon Zabulis[b], Thodoris D. Karapantsios[a,*]

[a] Division of Chemical Technology, School of Chemistry, Aristotle University, University Box 116, 541 24, Thessaloniki, Greece
[b] Institute of Computer Science, Foundation for Research and Technology, Hellas, N. Plastira 100 Vassilika Vouton, 700 13, Heraklion, Crete, Greece

GRAPHICAL ABSTRACT

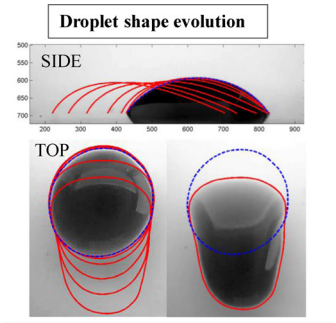

Side and top view of droplet motion under the influence of a tangential force

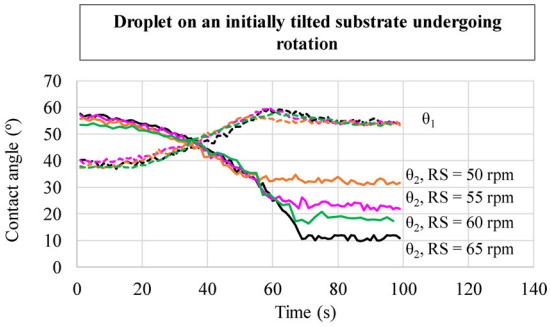

θ1, front and θ2, rear contact angles. RS, rotation speed

ARTICLE INFO

Keywords:
Forced wetting
Retention force
Tangential force
Droplet spreading/sliding
Centrifugal force
Non-axisymmetric droplets

ABSTRACT

Despite the extensive study of wetting in literature, there are still many unresolved issues regarding *forced wetting*. One of them refers to the effect of the initial droplet shape on the force required for spreading and sliding along a solid surface; an effect that has not ever been explicitly reported. Previous experimental works, in general, assume initially axisymmetric droplet shapes. In this study, experiments are performed with an innovative device, *Kerberos*, capable of subjecting sessile droplets at different tilting angles to varying centrifugal forces in order to explore the spreading/sliding behavior of droplets of different volumes and different initial shapes (including non-axisymmetric). A broad validation of the technique is achieved by the repeatability and consistency of measurements. Results for initially axisymmetric and non-axisymmetric droplets concerning contact angles, droplet length, droplet shape and velocity are presented and discussed. Furthermore, detailed results for the critical tangential accelerations required for the inception of spreading and sliding are presented showing the different sensitivity of these parameters on the droplet initial shape. Experimental results are employed to test the applicability of the well-known Furmidge equation for the retention force in the case of initially non-axisymmetric droplets. On this account, the initial length of droplets is found to be a more appropriate length scale in the Furmidge equation than the initial droplet width.

* Corresponding author.
E-mail address: karapant@chem.auth.gr (T.D. Karapantsios).

https://doi.org/10.1016/j.colsurfa.2018.04.004
Received 8 January 2018; Received in revised form 3 April 2018; Accepted 4 April 2018
Available online 12 April 2018

1. Introduction

Wetting represents the macroscopic manifestation of molecular interactions between liquids and solids in contact. In-depth understanding of wetting phenomena may lead the scientific community to develop more efficient processes (such as painting, printing, coating, washing, etc. [1]) in several technological fields (food, agriculture, oil, textile industries [2,3]). The great interest on the topic over the last decades has entailed massive research efforts focusing chiefly on the development of new experimental devices, methods and models to characterize wetting [4]. However, it seems that despite all these efforts, there are still many unresolved issues due to deficient experimental and theoretical protocols [5].

Wetting is a natural phenomenon arising when a liquid and a solid are brought together. However, wetting may also be forced to happen by the imposition of external body forces. In this case, the common term used in literature to describe the relevant phenomena is *forced wetting*. Hydrodynamic, mechanical or electrical forces may be applied to drive the system beyond the thermodynamic equilibrium [6,7]. Due to the large number of applications, many techniques and devices have been introduced for the study of forced wetting along the years. Nevertheless, these techniques present notable shortcomings. Some of them are related to inaccurate control of the forces applied to the system and to poor monitoring of the phenomena that leads to incomplete and, sometimes, controversial results [8,9].

Apart from the above, the study of wetting has focused almost exclusively on initially axisymmetric droplets. As a result, many of the principles governing wetting behavior have not been studied with the initial droplet shape being not axisymmetric. This is the case, for example, in describing the different stages of motion of a droplet along a surface. Concerning this point, when applying external forces, the movement of droplets occurs in two different sequential stages: spreading and sliding. On the one hand, the spreading stage happens when low forces are applied, and is provoked by the local instability of the droplet's front edge. This local instability causes the droplet's front edge to move in the direction of the force while the rear edge remains pinned to the solid. On the other hand, the sliding stage occurs when larger forces are applied and involves the global instability of the droplet, which causes the droplet to move all together in the direction of the force [10]. This phenomenon was reported for the first time by Bikerman in 1950 [11]. Regarding the influence of the initial contact angles on the spreading and sliding critical forces, Panchagnula [12] concluded that, in Tilted Plate experiments, the spreading angle was more sensitive to initial conditions than the sliding angle for axisymmetric droplets. However, it has never been tested if the different sensitivity between spreading and sliding angles would also exist with initially non-axisymmetric droplets.

Concerning specifically the sliding stage, multiple studies -using exclusively axisymmetric droplets- have tried to establish the different factors that play a role in the definition of the retention force F_s (or retentive force) [13], i.e. the minimum tangential force (parallel to the liquid/solid interface) required to induce droplet motion. A key concept to understand how the retention force is calculated is the contact angles hysteresis (CAH). Originally, Young [14] considered that for a liquid droplet resting on a horizontal surface, there is a force balance following the equation $\sigma_{sv} = \sigma_{sl} + \sigma_{lv}\cos\theta$ where σ_{sv} is the interfacial tension between solid and vapor, σ_{sl} is the interfacial tension between solid and liquid, σ_{lv} is the interfacial tension between liquid and vapor and θ is the equilibrium contact angle. Young's equation defined contact angle as a parameter to correlate the different thermodynamic interfacial tensions. However, Young contact angle θ (or equilibrium contact angle) cannot be easily achieved experimentally due to impurities and physical or chemical heterogeneities of the solid surface. The imperfections that lead the system away from the ideal case are manifested as contact angle hysteresis (CAH) [15]. CAH is therefore computed as the difference between the maximum and minimum contact angle that may arise from the liquid-solid contact. The upper limit of the contact angle is known as *advancing contact angle* (θ_A) and is formed as a droplet advances upon wetting the solid. The lower limit is the *receding contact angle* (θ_R), which appears during the dewetting process. After the deposition of a droplet on a surface, the contact angle ranges within these limits. When external forces are applied to a droplet, the value of CAH will determine if it remains pinned to the solid surface or not. The relation between CAH and the retention force F_s is explicitly expressed in Eq. (1), which was introduced by Furmidge in 1962 [13].

$$\frac{F_s}{\sigma R} = k(\cos\theta_R - \cos\theta_A) \tag{1}$$

where R is a value of the droplet's length scale, σ is the liquid-vapor surface tension ($\equiv\sigma_{sl}$), k is a proportionality factor known as *retention-force factor* and $(\cos\theta_R - \cos\theta_A)$ expresses the CAH. As evoked by Eq. (1), the relation between F_s and the CAH is mediated by the surface tension σ, by the droplet length scale R and by the retention-force factor k. Therefore, knowing the precise values of R and k would allow one to directly calculate the force necessary to achieve motion of any droplet with any CAH without the need of carrying out an experiment. Nevertheless, nowadays there is still no consensus on which geometrical feature of a droplet (length, width, radius, etc.) should represent R, from which the value of k can be derived. When the equation was originally proposed, the geometric feature of the droplet employed as R was the half-width of the droplet. In that case, it was considered that a sliding droplet could be approximated as a parallel-side elongated shape [13]. With the droplet's half-width value, Furmidge, derived a k value of 2. Later, Dussan supported the same value theoretically [16]. However, several later experiments under different conditions showed that using the droplet's half-width as R was not always adequate. Accordingly, instead of considering that the droplet had a parallel-sided elongated shape, later works proposed that the droplet kept its circular initial shape, and used the circle radius as R, and subsequently estimated k ($k = \pi$ [17]; $k = \pi/2$, [18]; $k = 4/\pi$ [19]). A more recent work [20] considered the droplet geometry to be accurately fitted by an ellipsoid and hence employed the ellipsoid equivalent radius as characteristic length (R) in the calculations obtaining $k = 48/\pi^3$. In brief, there is no consensus in literature on the geometrical feature that should be used to estimate k, and hence its precise characterization remains elusive, with reported values varying among studies. Furthermore, as mentioned above, the study of the retention forces involved in the sliding stage has only been examined with initially axisymmetric drops, and hence there is no evidence on how the different geometric features of non-axisymmetric drops (i.e. width versus length) affect the estimation of factor k. It is noted that Eq. (1) has been criticized to oversimplify the real physics of the problem [20]. However, despite the more advanced theories developed, it is still an indispensable tool for analyzing experimental data.

Finally, it is important to highlight that part of the disagreements in literature originate from methodological issues in the studies. For the determination of the retention force for droplet motion, and the respective droplet geometry, the tilted plate method has been employed in most of the cases [21,22]. In this method, a horizontal surface is gradually tilted until a critical inclination is reached. Henceforth, a droplet is not able to keep balance at the position of its initial deposition and slides along the surface in the direction of gravity. Although commonly used, the main disadvantage of the tilted plate technique concerns the maximum acceleration that can be imposed to a droplet, which is 1 g when the surface is completely vertical (tilted 90°). The maximum force that can be applied to a droplet is the one related to its own weight and, consequently, its use is restricted to large drops [19]. Another inconvenience comes from the inability to control independently tangential and normal forces. For this purpose, the use of the Rotating Disc technique, which uses centrifugal forces, was proposed [23,24]. Nevertheless, the techniques based only on centrifugal forces came along with a deficient monitoring of the phenomena. As the

substrate with the droplet was made to rotate while the camera was kept stationary, only one image for every rotation was acquired. In our lab, a device implementing this technique but with a camera rotating with the droplet was designed by Karapantsios et al. [25] with the aim of characterizing the stickiness (adhesiveness) of tomato pulp pastes with different solids and moisture content on solid substrates. Nowadays, the most advanced devices to study droplets' behavior are those combining the Tilted Plate and the Rotating Disc techniques. To our knowledge, the first device that allowed this combination was the Centrifugal Adhesion Balance (CAB; [26]). This device was successfully used to study how the time that a droplet rests on top of a surface prior to sliding [27] and the droplet size [28] affect the retention force. In the same line, Evgenidis et al. [29] combined the Tilted Plate and the Rotating Disc techniques to create *Kerberos*, an innovative device whose main functionality is the study of the evolution of the droplet shape under external body forces. The new device incorporates improvements related to the accurate control of forces acting on the system and to real time monitoring of the phenomena, and hence constitutes a state-of-the-art apparatus to investigate droplets behavior along the whole wetting process.

The aim of this work is two-fold: first, to explore if the difference in the sensitivity between sliding and spreading tangential forces found for initially axisymmetric droplets holds also for initially non-axisymmetric droplets. To this aim, we examine the tangential force required for the spreading and sliding of initially axisymmetric and non-axisymmetric droplets of different volumes under the action of gravity and centrifugal forces. Second, specifically for the sliding force, our aim is to examine which geometrical feature of the droplet should represent the R parameter in the Furmidge equation to obtain the best estimation of the retention-force factor k in the case of initially axisymmetric drops subjected to combined gravitational and centrifugal forces. All the experiments are carried out in *Kerberos*, a device that, as mentioned in the introduction, combines the rotation and tilting techniques to achieve accurate control of the tangential and normal forces acting on a droplet. It goes without saying that once meaningful data are produced under the herein examined relatively simple conditions, an effort will follow to develop an advanced theory to describe quantitatively the observed phenomena. The structure of the work is the following: At first the materials and procedures used are described in detail. Then the experimental data are presented and analyzed in order to wind up with specific answers to the questions raised above.

2. Materials and methods

2.1. Description of apparatus

The experiments were performed in *Kerberos*. *Kerberos* is a newly developed device that combines rotation and tilting to provide independent control of tangential and normal forces applied to a droplet lying on a solid substrate. The phenomena are monitored by 3 synchronized cameras rotating and tilting together with the droplet which are recording its shape and motion from a three-dimensional (X-Y-Z) perspective. The device comes along with a custom-made image analysis software that processes videos from the three cameras to determine a number of 2-dimensional droplet geometrical features as well as the 3-dimensional reconstruction of the droplet shape. From the latter, the distribution of contact angles around the droplet perimeter is estimated. The main features of *Kerberos* together with the principles of its operation and its capabilities were described in a previous work [29] along with preliminary results and a supporting theoretical model for the 2D shape of a droplet. It is noted that *Kerberos* can be used for dynamic studies (e.g. droplet motion during sliding, fast variation of applied forces) or static studies (slow variation of applying forces with respect to the hydrodynamic time scale).

In the present paper, only some essential features are mentioned as well as a few recent upgrades of the device. The rotating/tilting head of *Kerberos* is enclosed inside a cylindrical Plexiglas glove box that rotates with the substrate. The glove box keeps the enclosed air stagnant at controlled temperature/humidity and therefore suppresses evaporation of the droplet during rotation. Control of air temperature and humidity is implemented using an ultrasonic atomizer (Mini air humidifier LB.12, beurer) coupled to hot air blower (PD1600, Lafet). A Peltier element placed right under the thin copper sheet supporting the exchangeable substrate (solid surface under examination) allows the thermoregulation of the substrate independently from that of the enclosed air. This is necessary for non-isothermal wetting applications e.g., dropwise condensation. The deposition of droplets on the substrate is made using a 500 μL syringe (1750 LTN SYR, Hamilton) attached to a repeating dispenser (PB600-1, Hamilton, step 1/50 of syringe volume) that delivers a fixed liquid volume of 10 μL every time a button is pressed. Inside the glove box there is a special support which holds tightly the dispenser with the syringe during rotation.

The data acquisition system consists of three wireless cameras (WCB-100A, Brickcom) placed in orthogonal disposition (X-Y-Z) around the droplet. The cameras record the shape of the droplet from the top, side and back with a frame rate of 10 fps. The position of each camera can be adjusted in all three directions using micromanipulators in order to get the best shooting position every time. Recently, the magnifying capacity of the cameras has been enhanced by adding exchangeable lenses of different magnifying power (×7, ×14, ×21) (Olloclip, 3 in 1 Lens). Larger magnification can be used when very accurate data of droplet shape are required with the droplet being pinned to a fixed position on the substrate. On the other hand, if sliding experiments are performed, lenses with lower magnification power can be used to monitor the travel of the droplet over a longer distance. Cameras are calibrated against known lengths at the specific operating configuration every time (distance from droplet, magnifying lens).

The implementation of a new image analysis software is an important improvement since the first presentation of *Kerberos* [29]. The wireless cameras transmit images in real time and further store them in common format (.avi) for later processing. A custom-made software is developed in order to automatize the extraction of information from the video stream. Geometrical features of the 2D droplet, such as contact angles, coordinates of the edges and the highest point, coordinates of the whole shape (perimeter) contour are provided promptly in. xls or. txt format. Using this information, other parameters, such as droplet length, velocity and shape evolution, can be derived. Information from the three individual views (top, side and back) can be combined to compute a 3D reconstruction of the droplet surface. Measurements of 3D features (total droplet volume, local contact angles around the droplet perimeter) are correspondingly extracted. Due to space limitations, details of the 3D analysis and respective results will be presented in a subsequent publication. Supervisory Control and Data Acquisition software (SCADA) is implemented for the accurate regulation and synchronization of *Kerberos* operating parameters with the recorded videos.

2.2. Experimental procedure

As benchmark experiments for *Kerberos*, the forced wetting behavior of water droplets (ultrapure water, Direct-Q, Merck Millipore) over glass slides (known to be a well-behaved substrate) is studied. A low concentration of "brilliant blue" (0.5 g/L, Hina Dye Chem Industries) is added to the water in order to enhance the contrast of top view images of droplets. This increases the accuracy of image analysis leaving interfacial properties unaffected. Indeed, measurements of equilibrium and dynamic surface tension by the Wilhelmy plate (TE2, LAUDA) and maximum bubble pressure (BPA-1SX, Sinterface) methods showed no difference between the dyed and non-dyed water. The same holds for the values of advancing and receding contact angles as measured by *Kerberos*. Common microscope glass slides are used as substrate for the wettability tests. Glass slides are cleaned by immersion for 2 h in a

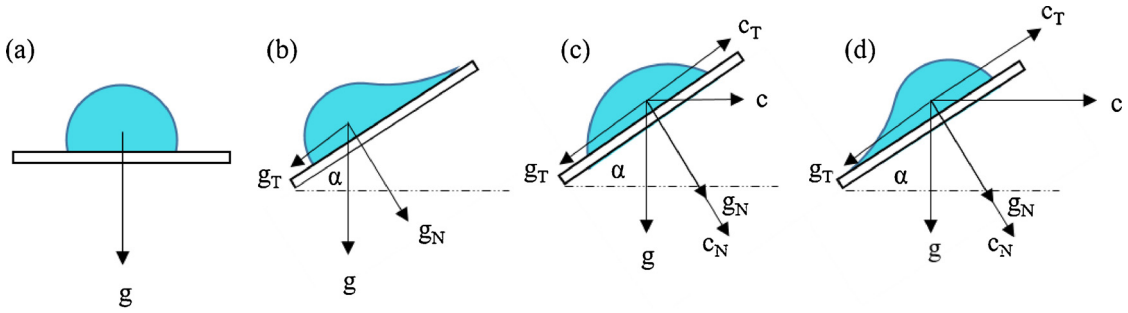

Fig. 1. Qualitative sketch of the combination of normal and tangential forces acting on a droplet lying on a substrate. (a) only gravitational forces at horizontal substrate, (b) only gravitational forces at a tilted substrate (initial condition prior to rotation), (c) gravitational forces plus low centrifugal forces at a tilted substrate, (d) gravitational forces plus high centrifugal forces at a tilted substrate.

solution of 60% nitric acid. Subsequently, slides are carefully rinsed with ultrapure water and dried in an oven at 100 °C for 1 h. The present experiments are conducted at 25 ± 2 °C and relative humidity 50 ± 5%.

Experiments are performed to explore the spreading/sliding behavior of droplets under centrifugal forces on horizontal and initially tilted substrates. Three droplet volumes are used in the experiments on horizontal substrate: 10, 20 and 30 μL. The substrate is then initially tilted to 3 different angles lower than the sliding angle (α_s) for the droplets of 20 μL ($\alpha_s = 45°$) and 30 μL ($\alpha_s = 35°$). Experiments with initial tilting are not performed for the 10 μL droplet because the detachment does not happen even for the maximum inclination of 90°. The initial tilting of the substrates provokes in some cases spreading of the droplet in the gravity direction but the rear part of the drop is always pinned in place. The tilting is performed in such direction that creates a tangential component opposite to the one of the centrifugal force as shown in Fig. 1.

The increasing rate for tilting and rotation speed is 1°/s and 1 rpm/s respectively. The angular speed ω is extracted from the experimental rotation speed (*RS*) adjusted in *Kerberos* for droplet sliding ($\omega = 2\pi \cdot f$, $f = {}^{RS}/_{60}$), r is the distance from the rotation axis to the droplet center (r = 25 cm for zero tilting) and α is the tilting angle of the substrate. The force balance on the system can be computed as follows for the different droplet volumes and tilting angles in the tangential (F_T, Eq. (2)) and normal direction (F_N, Eq. (3)) with respect to substrate:

$$F_T = m \cdot r \cdot \omega^2 \cdot \cos\alpha - m \cdot g \cdot \sin\alpha \quad (2)$$

$$F_N = m \cdot r \cdot \omega^2 \cdot \sin\alpha + m \cdot g \cdot \cos\alpha \quad (3)$$

The corresponding tangential and normal accelerations of the force field are computed by simply omitting mass (m) from the above relations. The experimental results are used to compute the retention-force factor (k) in Eq. (1) employing different geometric features of the droplet as R, the characteristic droplet length scale, for initially non-axisymmetric droplets.

3. Results and discussion

The critical rotation speeds for the inception of spreading and sliding on a horizontal plate are determined experimentally for three different droplet volumes 10, 20 and 30 μL. These speed values along with the corresponding tangential (centrifugal) accelerations are presented in Table 1 using the experimentally obtained angular speed ω and the distance between the drop and the axis of rotation (Tangential acceleration = $\omega^2 r$, $r = 25\,cm$). The accuracy in rotation values is ± 2 rpm reflecting chiefly the degree of repeatability.

Multiple repetitions are made for each set of experimental conditions to check the consistency of measurements resulting in a maximum variation of ± 2° in the front and rear contact angles. This refers to angles determined from the side-view camera. An example of

Table 1
Critical rotation speeds, RS, and tangential accelerations for spreading and sliding for three different droplet volumes on a horizontal substrate (*RS* ± 2 rpm).

Drop volume (μL)	Rotation speed (rpm)		Tangential acceleration (m/s^2)	
	Spreading	Sliding	Spreading	Sliding
10	54	70	7.67	12.90
20	38	58	3.96	9.22
30	27	50	2.00	6.85

experimental repeatability is shown in Fig. 2a where the different line types designate different experimental runs. The manual deposition of the droplet on the substrate often leads to droplets of slightly different initial shapes. In the present work, it is experimentally confirmed that the final advancing and receding contact angles are the same for droplets that slightly differ from the axisymmetric initial geometry, Fig. 2b.

Experiments are performed within the limits of spreading and sliding critical rotation speeds for a systematic exploration of the droplet shape evolution. Front and rear contact angles as well as the droplet elongation are computed for every case. For a 10 μL droplet, spreading begins at 54 rpm while sliding takes place at 70 rpm (Table 1). Consequently, experiments are performed for target rotation speeds of 55, 60, 65 and 70 rpm. The results are demonstrated in Fig. 2. In these and all later plots, the rotation speed is increased in a ramp at a rate of 1 rpm/s. Exploratory runs with rotational speed ramps as slow as 0.1 rpm/s give similar results so the present study can be considered as a static one (no influence of hydrodynamics).

Fig. 3a presents the evolution of the front (θ_1) and rear (θ_2) contact angles (in the direction of the force) with time. It is shown that, for all runs above the critical spreading rotation speed (54 rpm), the front edge of the droplet forms an angle with the solid surface which is equal to the advancing contact angle, θ_A (dashed lines). However, the rear edge of the droplet is pinned for rotation speeds under 70 rpm (solid lines). In these cases, the rear edge has not reached yet the value of the receding contact angle, θ_R. The rear angle decreases as the rotation speed increases until the receding angle value is reached at 70 rpm. At that rotation speed, the droplet detaches altogether from the surface and slides in the direction of the force.

Fig. 3b shows the rotation speed versus time in each experiment. The rotation speed increases at 1 rpm per second. As soon as the target speed is achieved, the rotation speed remains constant until the end of the experiment.

The advancement of the front edge, while the rear edge is pinned, induces droplet elongation which gets larger as the force increases and remains constant when the force is kept constant. Values of droplet length versus time for each rotation speed can be seen in Fig. 3c. As already mentioned, the manual droplet deposition leads to slightly different initial contact geometries corresponding to different initial

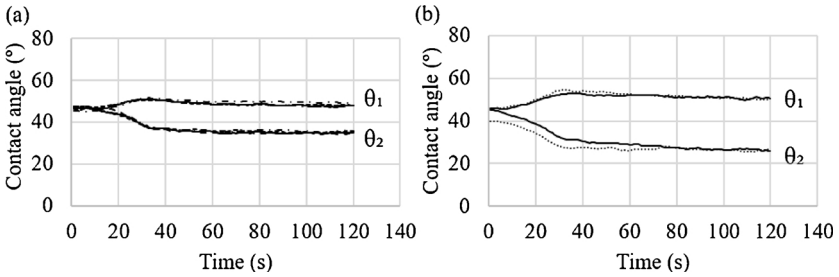

Fig. 2. (a) Front (θ_1) and rear (θ_2) contact angle versus time for four repetitions of the same experiment (20 μL droplet at 30 rpm on a horizontal substrate). The rotation speed is increased at 1 rpm/s rate until 30 rpm and then it is maintained constant. (b) Contact angles versus time for two experiments at the same conditions (30 μL droplet at 30 rpm on a horizontal substrate) starting with a symmetrical (solid line) and a slightly asymmetrical (dotted line) initial droplet shape. The rotation speed is increased with 1 rpm/s rate until 30 rpm and then it is maintained constant.

droplet lengths. In an effort to facilitate the comparison between the different droplet elongations for the different forces, Fig. 3d presents instantaneous droplet lengths normalized with regards to the respective initial droplet length.

Similarly to Fig. 3, Fig. 4 presents results for a 30 μL droplet with the rotation speed reaching values between 30 and 50 rpm. Once the droplet is set in motion, the advancing and receding contact angles are equal for the 10, 20 (see Fig. 7) and 30 μL droplet volume ($\theta_A = 55 \pm 2^\circ$, $\theta_R = 10 \pm 2^\circ$). The values of the advancing and receding contact angles are intrinsic to the liquid-solid pair. Therefore, when the droplet is large enough to overcome microscopic effects owing to surface heterogeneities, the aforementioned values do not depend on the droplet volume [30].

When applying an external force larger than the critical force for spreading to start, the droplet elongates in the direction of the force. The normalized elongation increases with the force for equivalent droplet volume, as shown in Figs. 3d and 4d.

The comparison of the evolution of droplet elongation for different droplet volumes (10, 20 and 30 μL) shows that larger droplets experience greater and faster elongation than smaller droplets (Fig. 5a). Normalized droplet length evolution is also provided for easier comparison of the obtained results, in Fig. 5b.

Experiments are also performed to determine the critical tangential acceleration required to move a droplet lying on a tilted substrate and presenting a non-circular initial contact area (footprint). These experiments are done with droplets of 20 and 30 μL. The employed tilting angles, α, are always below the angle value at which a droplet is observed to slide under solely the action of gravity. Moreover, the employed substrate tilting is such that the tangential component of the gravitational force acts in the opposite direction to the tangential component of the centrifugal force. A qualitative sketch of the acting forces was shown in Fig. 1. Thus, an increase of the initial tilting angle yields an increase of the centrifugal force that is necessary for droplet motion. Rotation speed values for sliding and spreading in these experiments are displayed in Table 2.

As it can be seen in Table 2, the change in the tangential acceleration for spreading for the different initial tilting is more prominent that the change in the tangential acceleration for sliding. In the case of the 20 μL droplet, the variation of the tangential acceleration computed as the ratio between the tangential acceleration for maximum and zero tilting is 1.10 and 2.1 for sliding and spreading, respectively. Based on these results, one may conclude that while the tangential acceleration required for sliding is hardly dependent on the initial symmetry, contrarily, the spreading acceleration is strongly related to the initial droplet shape. In the case that the initial droplet shape is non-axisymmetric and elongated, spreading starts at rotation speeds closer to sliding. Similarly, larger sensitivity of spreading than sliding was obtained in [12] using Tilted Plate for initially axisymmetric drops with varying initial contact angles.

Tilted plate experiments under the pure action of gravity reveal that for a 20 μL droplet the critical angle for the inception of spreading is 20° whereas the critical angle for the inception of sliding is 45°. Fig. 6 shows the experimental results for initial tilting of the substrate at 30°. The front (dashed lines) and rear (solid lines) contact angle evolution with time is presented in Fig. 6a. The droplet has spread after its initial deposition on the substrate due to the tilting employed prior to rotation. For this inclination of the substrate, droplet spreading takes place in the opposite direction to the tangential component of the centrifugal force. This is why the rear contact angles for all rotation speeds coincide with the value of the advancing contact angle before the rotation is initiated. The droplet goes through an axisymmetric shape at about $t = 60$ s ($RS = 55$ rpm) when the tangential components of gravitational and

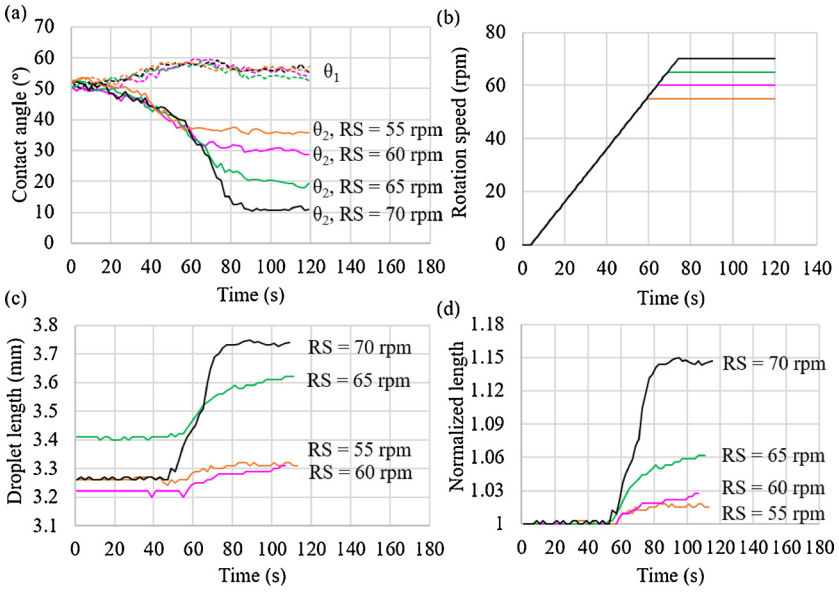

Fig. 3. Spreading/sliding behavior of a 10 μL droplet on a horizontal substrate for increasing rotation speed until different final rotation speeds (a) Front (dashed lines) and rear (solid lines) contact angles versus time. (b) Ramp increase of rotation speed versus time, 1 rpm/s. (c) Droplet length versus time. (d) Normalized droplet length versus time.

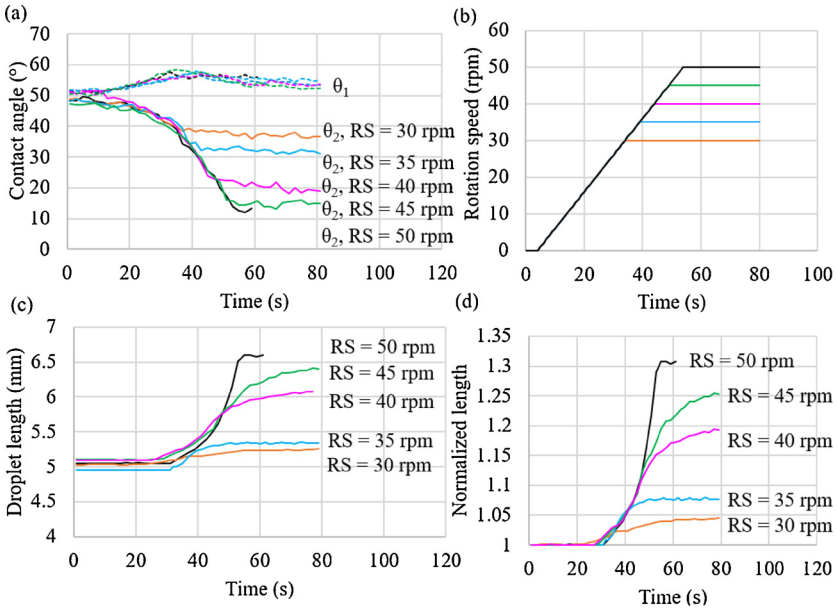

Fig. 4. Spreading/sliding behavior of a 30 µL droplet on a horizontal substrate for increasing rotation speed until different final rotation speeds (a) Front (dashed lines) and rear (solid lines) contact angles versus time. (b) Ramp increase of rotation speed versus time, 1 rpm/s. (c) Droplet length versus time. (d) Normalized droplet length versus time.

centrifugal forces offset each other (the front and rear angles coincide). The front contact angle (θ_1) evolves in all cases to eventually converge to the advancing contact angle while the values for the rear contact angle (θ_2) converge to the receding contact angle only when the rotation speed is 90 rpm. The centrifugal force is again increased as for the horizontal substrate experiments (1 rpm/s) and the target rotation speeds reached in each experiment can be seen in Fig. 6b. With the substrate tilted at 30°, sliding of the droplet occurs at 90 rpm whereas for the horizontal substrate sliding happens at 60 rpm. Fig. 6c shows that the initial droplet length is 5.1 ± 0.1 mm, while in the absence of initial tilting is 3.31 ± 0.1 mm. The corresponding normalized droplet length is presented in Fig. 6d.

Fig. 7 presents experimental results for a 30 µL droplet with an initial substrate tilting of 15°. Under purely the action of gravity, spreading of the droplet onsets at 10°. Thus, the droplet has already spread downwards the substrate before the rotation. For this, Fig. 7a shows that the initial rear angle (θ_2) corresponds to the advancing contact angle. In this experiment, the intersection point between front and rear contact angles, which corresponds to an axisymmetric droplet shape, occurs at about $t = 35$ s ($RS = 30$ rpm). Droplet detachment and sliding takes place at 65 rpm, whereas for the same droplet volume in the absence of initial tilting it happens at 50 rpm. The initial droplet length is 5.3 ± 0.1 mm (Fig. 7c), while it is 5 ± 0.05 mm for the same droplet volume on a horizontal substrate.

Fig. 8a compares the effect of the initial tilting on contact angles and droplet length for a 20 µL droplet. It is recalled that for a 20 µL droplet the critical tilting value for the inception of spreading is 20° and for the inception of sliding is 45°. This is the reason why for the experiments starting with 20° or 30° tilting, the initial contact angle in the rear part of the droplet is the corresponding advancing angle, $\theta_2 \sim 55°$. In the case of 10° initial tilting, the rear angle ($\theta_2 \sim 52°$) at the beginning of the experiment is between the angle for the horizontal substrate (approximately symmetrical drop, $\theta_2 \sim 48°$) and the advancing contact angle.

Table 2
Critical rotation speeds and tangential accelerations for spreading and sliding for two different droplet sizes and at different degree of initial tilting (RS ± 2 rpm).

Drop volume (µL)	Initial tilting α (°)	Rotation speed (rpm)		Tangential acceleration (m/s^2)	
		Spreading	Sliding	Spreading	Sliding
20	0	38	58	3.96	9.22
	10	47	66	3.89	9.33
	20	59	75	4.68	9.64
	30	75	87	6.85	10.91
30	0	27	50	2.00	6.85
	10	42	58	2.76	6.82
	15	49	63	3.27	7.10
	25	62	73	4.31	7.58

Fig. 8a also demonstrates that the final advancing and receding contact angles are alike (as expected), independently of the initial droplet symmetry. Fig. 8b presents the evolution of droplet length with increasing substrate tilting.

The velocity of both the front and rear droplet edges can be calculated from the differential variation of the edge positions with time. Fig. 9a and b shows the velocity of the front and rear droplet edges, respectively, for the same droplet volume and initial tilting of the

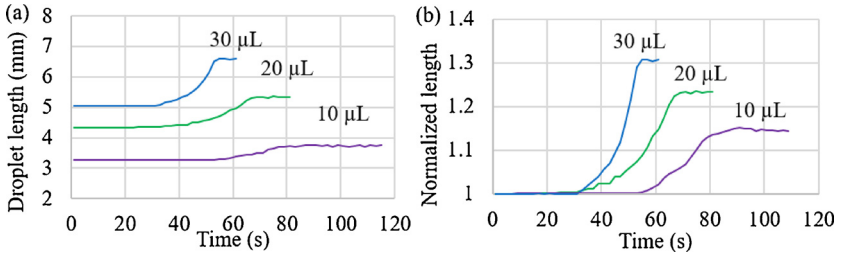

Fig. 5. (a) Evolution of droplet length versus time for the sliding of 3 different droplet volumes (10, 20 and 30 µL). (b) Corresponding normalized droplet length versus time.

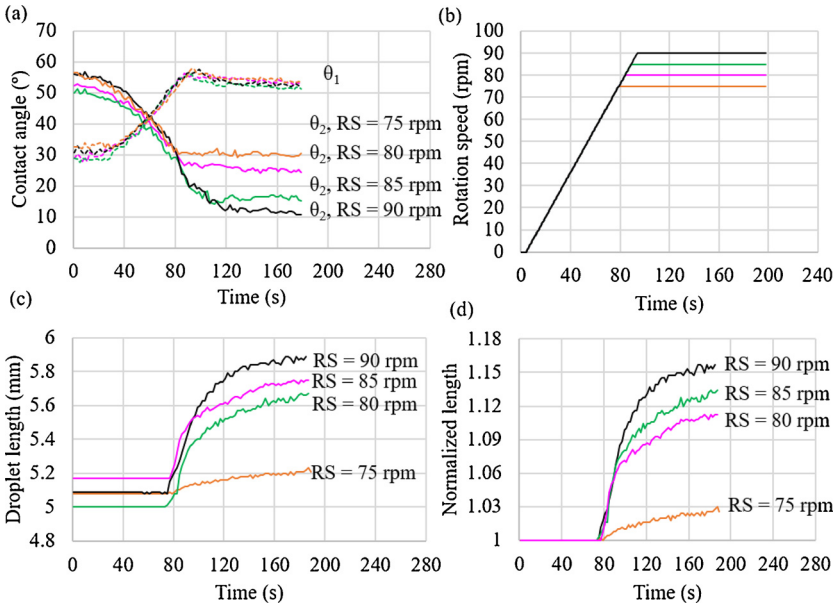

Fig. 6. Spreading/sliding behavior of a 20 μL droplet on a 30° initially tilted substrate for increasing rotation speed until different final rotation speeds (a) Front (dashed lines) and rear (solid lines) contact angles versus time. (b) Ramp increase of rotation speed versus time, 1 rpm/s. (c) Droplet length versus time. (d) Normalized droplet length versus time.

substrate (30 μL, 15°). According to Fig. 9a, the front edge seems to move at some moment for all examined rotation speeds because spreading is noticed in all cases. The peak of the droplet velocity is more pronounced for larger forces and appears at the time of maximum rotation speed. As soon as the maximum rotation speed is reached, it is kept constant until the end of the experiment. When the rotation speed stops increasing, the droplet does not move anymore and the speed of the front edge returns to zero except for the case of a sliding droplet, *RS* = 65 rpm, where it diverges until the droplet goes out of view. On the other hand, the rear edge is pinned for all cases except for the higher rotation speed that corresponds to a sliding droplet, Fig. 9b. The droplet speed for 65 rpm is divided by 5 for more convenient plotting of the results.

Processing of the acquired video streams provides also the side and top view contour points of the droplet shape. Inspection of the shape contour evolution with time enables a physical representation of the droplet shape deformation during spreading and sliding. Fig. 10 displays the evolution of the shape contours of a 20 μL droplet sliding at 60 rpm. These contours represent experimental top and side views for selected representative frames (time instants). At first, a spreading stage is noticed from the moving front edge and the pinned rear edge of the droplet. Next, as the force gradually increases the droplet detaches from the substrate and slides in the direction of the force.

Fig. 11 shows the spreading of a 30 μL droplet at 30 rpm. In the latter, the droplet has its rear edge always pinned and elongates in the direction of the force.

3.1. Estimation of retention-force factor k

For the estimation of the retention-force factor, *k*, the Furmidge equation previously introduced is arranged as follows:

$$k \cdot R = \frac{F_s}{\sigma \cdot (\cos\theta_R - \cos\theta_A)} \tag{4}$$

where the retention force F_S is the applied tangential force at the moment of sliding inception which is computed using the balance of forces, Eq. (2) shown in Fig. 1.

Having the value of F_s from the experiments, the product *kR* is easily

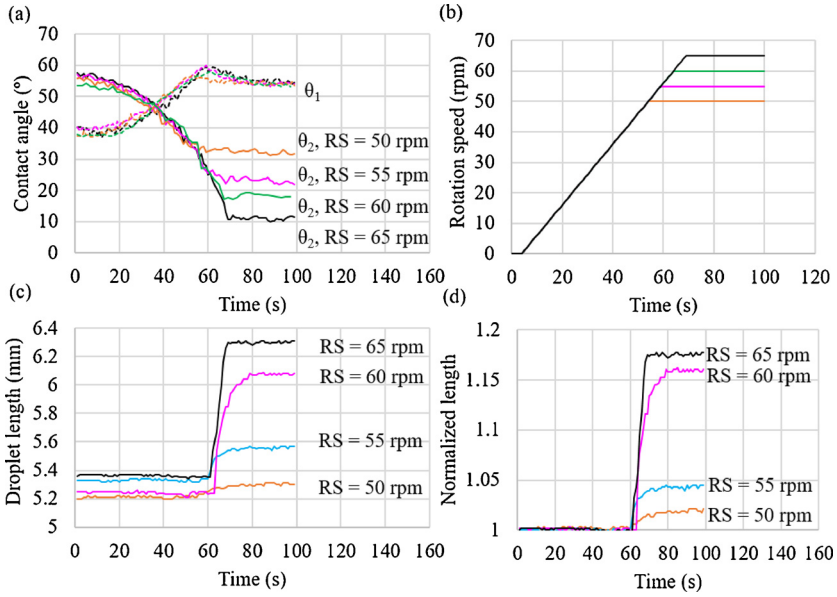

Fig. 7. Spreading/sliding behavior of a 30 μL droplet on a 15° initially tilted substrate for increasing rotation speed until different final rotation speeds (a) Front (dashed lines) and rear (solid lines) contact angles versus time. (b) Ramp increase of rotation speed versus time, 1 rpm/s. (c) Droplet length versus time. (d) Normalized droplet length versus time.

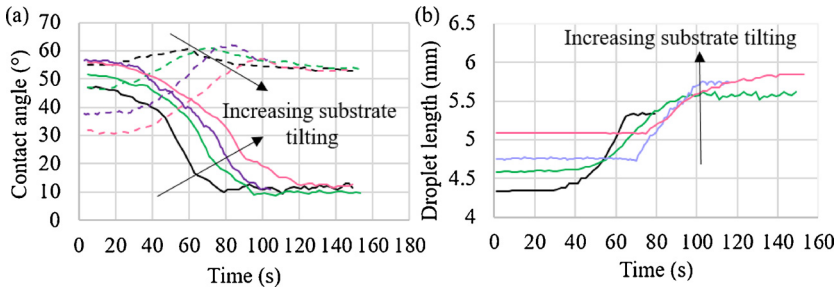

Fig. 8. Comparison of the evolution of (a) front (dashed line) and rear (solid line) contact angles and (b) droplet lengths versus time for a 20 µL drop on a different initially tilted substrate (0°, 10°, 20° and 30°).

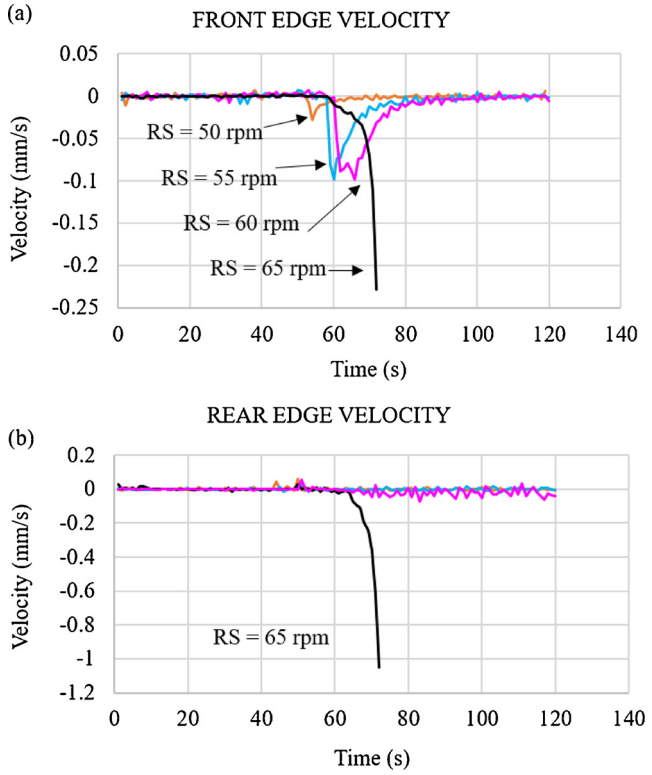

Fig. 9. Velocity of the front and rear edges of a 30 µL droplet at 15° initially tilted substrate. For convenience in presentation, the velocity of the rear edge at 65 rpm is divided by 5 in the plot.

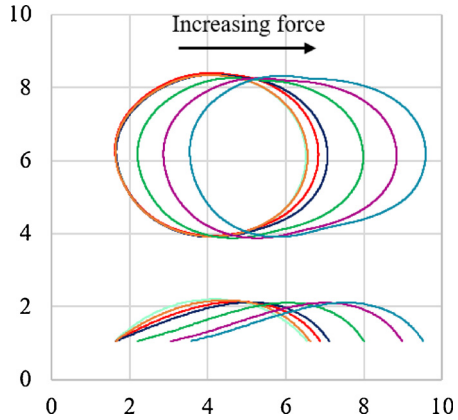

Fig. 10. Top (upper) and side (lower) view of the experimental contour evolution during the sliding of a 20 µL droplet at 50 rpm on a horizontal substrate.

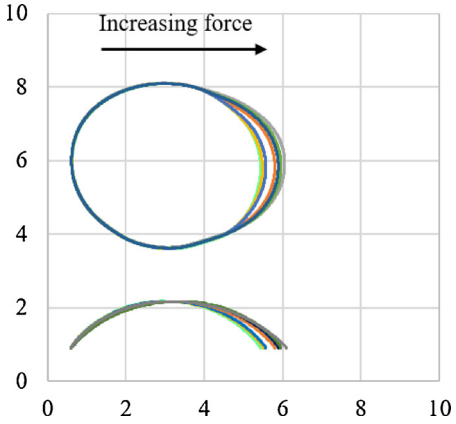

Fig. 11. Top (upper) and side (lower) view of the experimental contour evolution during the spreading of a 30 µL droplet at 30 rpm on a horizontal substrate. Fig. 12. Droplet initial geometry (length and width) from top view for a 20 µL drop placed on (a) horizontal substrate, (b) initial substrate tilting of 20°, (c) initial substrate tilting of 30°.

Table 3
Values of the retention-force factor,*k*, for three droplet volumes, *V* (10, 20 and 30 µL) at various initial substrate tilts, *α* (0°–30°) derived for different droplet length scales: droplet initial width (k_1), initial length (k_2), and sliding length (k_3). *FDS*: fractional degree of scatter (max-min/average).

V (µL)	α (°)	Initial width (mm)	k_1	Initial Length (mm)	k_2	Sliding length (mm)	k_3
10	0	4.09	1.07	4.10	1.06	4.70	0.93
20	0	5.40	1.02	5.40	1.02	6.54	0.84
30	0	6.03	1.02	6.15	1.00	6.86	0.89
20	10	5.48	1.01	5.50	1.01	6.70	0.83
20	20	5.60	1.04	6.03	0.97	6.60	0.88
20	30	5.70	1.14	6.45	1.00	6.72	0.97
30	10	5.90	1.03	6.37	0.96	6.93	0.88
30	15	5.84	1.09	6.45	0.99	6.83	0.93
30	25	6.02	1.15	7.00	0.99	7.10	0.98
Average			1.07		1.02		0.91
FDS			0.13		0.10		0.16

computed using Eq. (4) where the values for the advancing θ_A and receding θ_R contact angles are taken as the average of experimental measurements. R is a length scale extracted from droplet geometry. Several values of R have been proposed in literature. Most of them refer to the droplet geometry at the moment of sliding inception (e.g. droplet radius, droplet width, some kind of droplet average dimension, etc.). In this work, we consider three different choices for R for the calculation of k_1, k_2 and k_3: (1) initial droplet width, (2) initial droplet length and (3) sliding droplet length. The computed values of k_i's are shown in Table 3 along with the fractional degree of scatter (*FDS*) calculated as the difference between the maximum and minimum value of k_i divided by the average k_i value. Although the FDS difference among the three

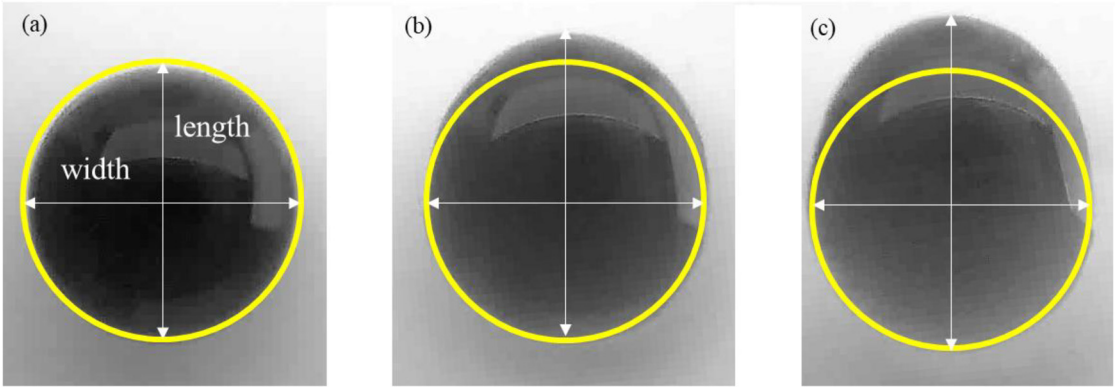

Fig. 12. Droplet initial geometry (length and width) from top view for a 20 μL drop placed on (a) horizontal substrate, (b) initial substrate tilting of 20°, (c) initial substrate tilting of 30°.

considered length scales is not large, the droplet initial length appears to be the best option based not only on the criterion of minimum FDS but also because there is no correlation between calculated k_2 values and initial tilting angle α.

As shown in Table 3, the initial width is pretty constant (within experimental error) for the same droplet volume for both axisymmetric and non-axisymmetric droplets leading to a continuous increasing k with tilting. On the contrary, the initial droplet length seems more appropriate because it increases with increasing tilting (as the retention force does) leading to the derivation of a quite constant value of k.

In Fig. 12, the initial droplet shape is shown for a 20 μL droplet in (a) horizontal substrate, (b) initial substrate tilting of 20° and (c) initial substrate tilting of 30°. For the case (a) the use of width and length is indifferent (aspect ratio β = length/width = 1). However, for droplets with initial aspect ratio higher than 1 (non-axisymmetric droplets), the droplet length appears to be a better choice for the characteristic length in the retention force calculation. A generalization of the above observation is that the initial shape of droplets (before the application of the force that eventually will lead to sliding) must be used for the computation of k value (implying a fundamental connection between retention force and droplet length). The scatter in the k_2 values is random and compatible with the stated repeatability and accuracy of rotation speed for sliding. On the other hand, the values of k_1 are strongly correlated with the initial angle α (i.e. initial droplet deformation). The scatter of k_3, which is the largest of all, exhibits also a correlation with the initial tilting. Thus, the present work suggests that, for non-axisymmetric droplets, Eq. (1) holds to a satisfactory degree if one uses the initial droplet length as the length scale R with the value of $k = 1$. This result is compatible with the values of $k = 2$ proposed by previous authors [13,16] bearing in mind that in those studies, the half-width was used instead of the whole width or length.

4. Conclusions

This work presents some new results obtained using *Kerberos,* an innovative device that allows the study of droplet spreading/sliding under independent control of gravitational and centrifugal forces. The technique is shown to offer good repeatability and stability (yielding the same advancing and receding contact angles for any initial droplet shape). Several experimental scenarios are investigated for the system water-glass considering different droplet volumes, rotation speeds and tilting angles of the solid substrate (e.g. consideration of initially non-axisymmetric drops). The evolution of the front and rear contact angles and the droplet length is presented along with the rotation speeds necessary for droplet spreading and sliding. Evolution of the droplet's top and side shape contour offers a direct physical representation of droplet deformation during spreading and sliding. It is found that the degree of the deviation of droplet shape from axisymmetry influences more the force required for spreading than for sliding. In addition, it is found that the Furmidge equation for droplet sliding inception can be extended to initially non-axisymmetric droplets by simply considering the initial droplet length as characteristic length scale. Conclusively, *Kerberos* seems to have the potential to facilitate the understanding of several unresolved issues regarding forced wetting phenomena.

Acknowledgements

This work was supported by Marie-Curie ITS "Complex wetting Phenomena, CoWet" (FP7-PEOPLE-2013-ITN, grant number 607861) and by MAP Project "Enhanced Condensers in Microgravity, ENCOM-3" (European Space Agency, Contract No.: 4200020276) and was carried out under the umbrella of COST Action MP1305 "Flowing Matter". We thank Mr. Triantafyllos Tsilipiras, Mr. Kostas Zacharias and Mr. Elias Paphianos for their technical support in upgrading Kerberos.

References

[1] J. Kim, M.W. Moon, K.R. Lee, L. Mahadevan, H.Y. Kim, Hydrodynamics of writing with ink, Phys. Rev. Lett. 107 (2011) 2–5, http://dx.doi.org/10.1103/PhysRevLett.107.264501.
[2] S. Li, J. Huang, Z. Chen, G. Chen, Y. Lai, A review on special wettability textiles: theoretical models, fabrication technologies and multifunctional applications, J. Mater. Chem. A 5 (2017) 31–55, http://dx.doi.org/10.1039/C6TA07984A.
[3] N.R. Morrow, Wettability and its effect on oil recovery, Soc. Pet. Eng. J. 42 (1990) 1476–1484, http://dx.doi.org/10.2118/21621-PA.
[4] O. Arjmandi-Tash, N.M. Kovalchuk, A. Trybala, I.V. Kuchin, V. Starov, Kinetics of wetting and spreading of droplets over various substrates, Langmuir 33 (2017) 4367–4385, http://dx.doi.org/10.1021/acs.langmuir.6b04094.
[5] Y.D. Shikhmurzaev, Some dry facts about dynamic wetting, Eur. Phys. J. Spec. Top. 197 (2011) 47–60, http://dx.doi.org/10.1140/epjst/e2011-01435-x.
[6] L. Espín, S. Kumar, Droplet wetting transitions on inclined substrates in the presence of external shear and substrate permeability, Phys. Rev. Fluids 2 (2017) 14004, http://dx.doi.org/10.1103/PhysRevFluids.2.014004.
[7] A. Hemmi, S. Muff, O. Gröning, S. De Feyter, J. Osterwalder, S.F.L. Mertens, T. Greber, Switching stiction and adhesion of a liquid on a solid, Nature 534 (2016) 676–679, http://dx.doi.org/10.1038/nature18275.
[8] C. Della Volpe, S. Siboni, Use, abuse, misuse and proper use of contact angles: a critical review, Rev. Adhes. Adhes. 3 (2015) 365–385, http://dx.doi.org/10.7569/RAA.2015.097310.
[9] A. Marmur, C. Della Volpe, Contact angles and wettability: towards common and accurate terminology, Surf. Innov. 5 (2017) 3–8, http://dx.doi.org/10.1680/jsuin.17.00002.
[10] V. Berejnov, R.E. Thorne, Effect of transient pinning on stability of drops sitting on an inclined plane, Phys. Rev. E – Stat. Nonlinear Soft Matter Phys. 75 (2007) 1–6, http://dx.doi.org/10.1103/PhysRevE.75.066308.
[11] J.J. Bikerman, Sliding of drops from surfaces of different roughnesses, J. Colloid Sci. 5 (1950) 349–359, http://dx.doi.org/10.1016/0095-8522(50)90059-6.
[12] N. Janardan, M.V. Panchagnula, Effect of the initial conditions on the onset of motion in sessile drops on tilted plates, Colloids Surf. A Physicochem. Eng. Asp. 456 (2014) 238–245, http://dx.doi.org/10.1016/j.colsurfa.2014.05.051.
[13] C.G.L. Furmidge, Studies at phase interfaces. I. The sliding of liquid drops on solid surfaces and a theory for spray retention, J. Colloid Sci. 17 (1962) 309–324, http://dx.doi.org/10.1016/0095-8522(62)90011-9.
[14] T. Young, An essay on the cohesion of fluids, philos, Trans. R. Soc. Lond. 95 (1805) 65–87, http://dx.doi.org/10.1098/rstl.1805.0005.

[15] D.Y. Kwok, a.W. Neumann, Contact angle measurement and contact angle interpretation, Adv. Colloid Interface Sci. 81 (1999) 167–249, http://dx.doi.org/10.1016/S0001-8686(98)00087-6.
[16] E.B. Dussan V, The moving contact line: the slip boundary condition, J. Fluid Mech. 77 (1976) 665–684, http://dx.doi.org/10.1017/S0022112076002838.
[17] E. Wolfram, R. Faust, Contact angle hysteresis and the young contact angle, in: J.F. Padday (Ed.), Wetting, Spreading Adhes, Academic Press, London, 1978, pp. 213–222.
[18] R.A. Brown, F.M. Orr, L.E. Scriven, Static drop on an inclined plate: analysis by the finite element method, J. Colloid Interface Sci. 73 (1980) 76–87, http://dx.doi.org/10.1016/0021-9797(80)90124-1.
[19] C.W. Extrand, A.N. Gent, Retention of liquid drops by solid surfaces, J. Colloid Interface Sci. 138 (1990) 431–442, http://dx.doi.org/10.1016/0021-9797(90)90225-D.
[20] A.I. ElSherbini, A.M. Jacobi, Retention forces and contact angles for critical liquid drops on non-horizontal surfaces, J. Colloid Interface Sci. 299 (2006) 841–849, http://dx.doi.org/10.1016/j.jcis.2006.02.018.
[21] G. Macdougall, C. Ockrent, Surface energy relations in liquid/solid systems. I. The adhesion of liquids to solids and a new method of determining the surface tension of liquids, Proc. R. Soc. A Math. Phys. Eng. Sci. 180 (1942) 151–173, http://dx.doi.org/10.1098/rspa.1942.0031.
[22] B. Krasovitski, A. Marmur, Drops down the hill: theoretical study of limiting contact angles and the hysteresis range on a tilted plate, Langmuir 21 (2005) 3881–3885, http://dx.doi.org/10.1021/la0474565.
[23] R. Goodwin, D. Rice, S. Middleman, A model for the onset of motion of a sessile liquid drop on a rotating disk, J. Colloid Interface Sci. 125 (1988) 162–169, http://dx.doi.org/10.1016/0021-9797(88)90065-3.
[24] K. Katoh, M. Higashine, T. Wakimoto, R. Masuda, On the sliding and profile of a liquid droplet on a rotating disk, Heat. Transf. – Asian Res. 39 (2010) 59–75, http://dx.doi.org/10.1002/htj.20276.
[25] A.M. Goula, T.D. Karapantsios, K.G. Adamopoulos, An advanced centrifugal technique to characterize the sticking properties of tomato pulp during drying, Dry Technol. 25 (2007) 599–607, http://dx.doi.org/10.1080/07373930701227151.
[26] R. Tadmor, P. Bahadur, A. Leh, H.E. N'Guessan, R. Jaini, L. Dang, Measurement of lateral adhesion forces at the interface between a liquid drop and a substrate, Phys. Rev. Lett. 103 (2009) 1–4, http://dx.doi.org/10.1103/PhysRevLett.103.266101.
[27] R. Tadmor, K. Chaurasia, P.S. Yadav, A. Leh, P. Bahadur, L. Dang, W.R. Hoffer, Drop retention force as a function of resting time, Langmuir 24 (2008) 9370–9374, http://dx.doi.org/10.1021/la7040696.
[28] P.S. Yadav, P. Bahadur, R. Tadmor, K. Chaurasia, A. Leh, Drop retention force as a function of drop size, Langmuir 77710 (2008) 3181–3184, http://dx.doi.org/10.1021/la702473y.
[29] S.P. Evgenidis, K. Kalić, M. Kostoglou, T.D. Karapantsios, Kerberos: a three camera headed centrifugal/tilting device for studying wetting/dewetting under the influence of controlled body forces, Colloids Surf. A Physicochem. Eng. Asp. (2016) 1–32, http://dx.doi.org/10.1016/j.colsurfa.2016.07.079.
[30] J. Drelich, The effect of drop (bubble) size on contact angle at solid surfaces, J. Adhes. 63 (1997) 31–51, http://dx.doi.org/10.1080/00218469708015212.